Shaft resistance of driven cast-in-situ piles in sand

Cite as:

Flynn, K.N. and McCabe, B.A. (2016) Shaft resistance of driven cast-in-situ piles in sand, *Canadian Geotechnical Journal*, Vol. 53, No. 1, pp. 49-59.

DOI: 10.1139/cgj-2015-0032

THE SHAFT RESISTANCE OF DRIVEN CAST-IN-SITU PILES IN SAND

Kevin N. Flynn BA BAI PhD[1]

Bryan A. McCabe BA BAI PhD[2*]

[1]Geotechnical Engineer, AGL Consulting, Sandyford, Dublin 18, Ireland; formerly PhD Candidate, College of Engineering & Informatics, National University of Ireland, Galway, Ireland. e-mail: kevin.flynn@agl.ie

[2]Lecturer, College of Engineering & Informatics, National University of Ireland, Galway, Ireland

[*]Corresponding author, e-mail: bryan.mccabe@nuigalway.ie, telephone: +353-91-492021

KEYWORDS

Driven; cast-in-situ; piles; sand; shaft resistance; friction fatigue

WORDCOUNT

5461

ABSTRACT

Driven cast-in-situ (DCIS) piles are classified as a large displacement pile, despite sharing certain aspects of their construction with replacement pile types. However, there are relatively few case histories of load tests on DCIS piles in the literature to verify the assumption that they behave as large displacement piles. In particular, the shaft resistance of DCIS piles in sand is uncertain due to the complex interaction between the freshly-cast concrete and surrounding displaced soil after extraction of the steel installation tube. This paper describes the installation, curing and maintained compression load testing of three temporary-cased DCIS test piles at a uniform sand site near Coventry, United Kingdom. The piles were instrumented with vibrating wire strain gauges to enable accurate measurement of the local shear stress generated on the pile shaft during maintained compression loading. The tests showed that the peak average and local shear stresses tended to mobilise at greater shaft displacements than traditional preformed displacement piles during loading. A clear reduction in normalised local shear stresses (and hence radial effective stress) at failure with distance from the pile base, i.e. friction fatigue, was evident for all piles, implying that radial stresses generated during driven installation of the steel tube are not erased upon concreting and tube withdrawal. Furthermore, the inferred normalised radial effective stresses at failure were remarkably similar to those reported for traditional preformed displacement piles in the literature.

INTRODUCTION

Driven cast-in-situ (DCIS) piles are a viable alternative to traditional pile types due to the potential to match their lengths to the depth of penetration required (Fleming et al. 2007; Tomlinson and Woodward 2008) and therefore offer considerable savings in terms of both construction time and costs for large-scale piling projects. The installation process of a temporary-cased DCIS pile, illustrated in Figure 1, involves top-driving a hollow steel tube with a sacrificial circular steel plate placed at the base of the tube in order to prevent ingress of soil and water during driving. When the tube reaches the required depth of penetration, the hammer is retracted and the pile is subsequently constructed by pouring concrete into the installation tube via a special skip. Alternatively, the concrete can be pumped into the tube using a specialised connection fitted to the head of the tube. When concreting is complete, the hammer is reattached and the tube is extracted from the soil, with several blows applied to the tube during this process in order to eliminate any voids present in the concrete. Reinforcement may be placed either before or after concreting. The pile is then left to cure in-situ for a number of days, with the steel plate remaining at the base.

While aspects of the DCIS pile construction process are shared with replacement pile types (i.e. casting of concrete in-situ and the resulting rough shaft interface), the use of driving to install DCIS piles has led to their classification as large displacement piles (BSI 1986) and practitioners have consequently tended to resort to traditional displacement pile design methods when estimating the shaft and base capacity of DCIS piles in sand (Tomlinson and Woodward 2008). Flynn et al. (2014) have used a small database of 16 DCIS piles with adjacent CPT data to demonstrate that CPT-based displacement design methods are relatively successful in estimating the capacity of DCIS piles in sand. However, there are relatively few case histories of load tests in the literature, and given the complex interaction between the freshly-cast concrete and the surrounding displaced soil after tube extraction, a systematic investigation of the shaft behaviour of DCIS piles in sand is warranted.

The results of a maintained compression load test on a 320 mm diameter, 5.75 m long instrumented DCIS pile (designated Pile S1) in a uniform sand deposit at a site in Shotton, Wales by Flynn et al. (2013) showed that the pile behaved in a predominantly end-bearing manner during loading, with local shear stresses reducing with increasing distance from the base. The results of this work prompted the comprehensive study described in this paper in which three DCIS piles were installed, cured and subjected to maintained compression load tests in a uniform sand deposit near Coventry, United Kingdom. Each test pile was instrumented with vibrating wire strain gauges at a four separate levels to enable accurate measurement of the local shear stresses during loading. The results are subsequently compared with the findings of similar studies for preformed displacement piles, with particular emphasis given to the potential influence of friction fatigue on the local shear stresses mobilised on the test piles during loading.

BACKGROUND

The local shear stress at failure τ_{sf} of a displacement pile in sand is traditionally expressed using the following equation, based on conventional earth pressure theory:

$$\tau_{sf} == K_f \sigma'_{v0} \tan \delta_f \qquad \text{Eqn. 1}$$

where K_f is the lateral earth pressure coefficient at failure, σ'_{v0} is the vertical effective stress and δ_f is the interface friction angle at failure. The lateral earth pressure coefficient K_f depends on several factors, including the level of soil displacement during installation and in-situ soil state. For DCIS piles, Fleming et al. (2007) suggest that K_f values in excess of 1.2 are possible during driving of the steel installation tube, but reductions in radial effective stress will inevitably occur after tube extraction as the freshly-cast concrete interacts with the surrounding displaced soil, with K_f = 1.0 subsequently recommended for design purposes. Despite the simplicity of the lateral earth pressure approach, the use of a constant K_f value implies a linear relationship between local shear stress and vertical effective stress, which is in contrast with observations of shaft resistance during loading of

instrumented displacement piles in the field (Randolph et al. 1994). Furthermore, reviews of pile design methods over the years have highlighted the relatively poor performance of earth pressure methods in predicting displacement pile capacity (Briaud and Tucker 1988; Toolan et al. 1991; Schneider et al. 2008).

Undoubtedly the most extensive observations of displacement pile behaviour in sand were obtained by researchers at Imperial College London over a 10 year period beginning in the late 1980s as part of a comprehensive research programme geared towards offshore applications. Pile tests were conducted in loose to medium dense sand at Labenne (Lehane 1992; Lehane et al. 1993) and dense sand at Dunkirk (Chow 1997) using a 102 mm diameter, closed-ended steel model pile (referred to as the Imperial College Pile or ICP) with instrumentation clusters at several levels near the pile tip, enabling near-continuous measurements of radial and local shear stresses, axial loads and pore pressures during installation, equalisation and loading. The results of the ICP tests demonstrated that the local shear stress of displacement piles in sand obeys the Coulomb failure criterion:

$$\tau_{sf} = \sigma'_{rf} \tan\delta_f = \left(\sigma'_{rc} + \Delta\sigma'_{rd}\right)\tan\delta_{cv} \qquad \text{Eqn. 2}$$

where σ'_{rf} is the radial effective stress at failure, σ'_{rc} is the radial effective stress after installation and equalisation, $\Delta\sigma'_{rd}$ is the change in radial stress due to interface dilation during loading and δ_{cv} is the constant-volume interface friction angle. The profiles of radial effective stress at each sensor level between installation jacking strokes closely resembled the corresponding measured cone resistance q_c profiles but reduced systematically at a given distance h from the pile base with increasing pile embedment. This phenomenon, known as 'friction fatigue' (Heerema 1980), is a consequence of the densification of the shear band at the pile-soil interface during the cyclic process of driven and/or jacked installation (Randolph 2003). A series of centrifuge pile installation tests performed by White and Lehane (2004) demonstrated that the rate of degradation in radial stress was strongly dependent on the number of shearing cycles N during installation and loading. This trend was

confirmed by Gavin and O'Kelly (2007) who conducted a series of installation tests in a dense over-consolidated sand deposit using a 73 mm diameter closed-ended steel pile equipped with radial stress sensors at several sections of the pile shaft. Despite the strong relationship between the number of shearing cycles N during installation and the rate of degradation in radial stress, existing design approaches tend to model friction fatigue as a function of normalised distance from the base h/D (where D is the pile diameter). A review of over 70 high-quality load tests on instrumented driven piles in sand by Lehane et al. (2005b) resulted in the following best-fit expression for the degradation in stationary radial stress after installation for *driven* closed-ended displacement piles:

$$\sigma'_{rc} = 0.03 q_c \left(\frac{h}{D} \right)^{-0.5} \qquad \text{Eqn. 3}$$

Changes in radial stress during loading are attributed to constrained dilation of the sand particles at the pile-soil interface under the action of shearing and vary with stress level, density and interface roughness (Lehane and White 2005). Using the results of the ICP tests at Labenne and a limited number of case histories of displacement pile behaviour in sand reported in the literature, Lehane and Jardine (1994) showed that dilation-related changes in radial stress can be reasonably predicted using the following expression developed by Boulon and Foray (1986) based on cavity expansion theory:

$$\Delta\sigma'_{rd} = \frac{4G\Delta y}{D} \qquad \text{Eqn. 4}$$

where $\Delta\sigma'_{rd}$ is the increase in radial stress due to interface dilation, G is the operational shear stiffness of the sand mass constraining dilation, Δy is radial displacement of shear band and D is the pile diameter. Equation 4 implies that $\Delta\sigma'_{rd}$ is inversely proportional to pile diameter, thus providing an explanation for the higher values of shaft friction typically observed on model-scale piles in comparison to field-scale piles. For example, tension tests conducted on centrifuge model piles in sand by Lehane et al. (2005a) showed large variations in average shear stress $\tau_{s,avg}$ with minor

changes in model pile diameter. To date, changes in radial stress during loading of full-scale piles in the field have only been obtained for preformed displacement piles (i.e. precast concrete and steel pile types), with reliable measurements of radial stresses in cast-in-situ pile types significantly hampered by difficulties associated with the placement of radial stress sensors in a pile which is constructed in-situ by concreting. Consequently, radial stresses are typically inferred from measurements of local shear stresses using Equation 2. Gavin et al. (2009) examined the influence of interface dilation on the shaft resistance of two instrumented continuous flight auger (CFA) piles installed in sand at a site in Killarney, Ireland. The two test piles, designated P450 and P800, had nominal diameters of 450 mm and 800 mm respectively, and were subjected to maintained compression load tests after a suitable curing period. Despite the contrasting diameters, the piles exhibited near-identical profiles of peak average shear stress, implying that interface dilation was negligible during loading.

The various high-quality studies of displacement pile behaviour in sand conducted in recent years have led to the development of several CPT-based design methods which have been shown to provide improved predictions of shaft capacity for displacement piles in sand in comparison to traditional design methods (Jardine et al., 2005; Schneider et al. 2008). For example, the University of Western Australia UWA-05 method (Lehane et al. 2005b) recommends the use of Equations 2, 3 and 4 to estimate the shaft resistance of closed-ended displacement piles in siliceous sand.

The applicability of the mechanisms governing the shaft resistance of preformed closed-ended displacement piles to DCIS piles remains unverified. The development of friction fatigue during DCIS pile installation is conceivable, as the soil surrounding the pile is likely subjected to extreme loading cycles during driven installation of the steel tube. As noted by Fleming et al. (2007), however, extraction of the tube results in a complex interaction between the freshly-cast concrete

and surrounding soil. In light of such uncertainties surrounding the shaft resistance of DCIS piles in sand, a series of maintained compression load tests were performed on three instrumented DCIS piles installed in a uniform sand deposit near Coventry, United Kingdom.

GROUND CONDITIONS

The instrumented pile tests were conducted at a uniform sand deposit on the outskirts of the village of Ryton-on-Dunsmore, approximately 8 km southeast of Coventry in Warwickshire, United Kingdom. The geology of the Warwickshire area comprises Triassic Mercia Mudstone bedrock which is overlain by glacial deposits of clay, sand and gravel; the formation of these deposits is described extensively by Shotton (1953). The majority of the Ryton-on-Dunsmore area (including the test site) is underlain by a uniform deposit of brown sand, known locally as Baginton Sand.

Cone penetration tests (CPT) were undertaken to establish the ground conditions at the test site. A total of three CPTs were conducted using a 36 mm diameter piezocone which penetrated to maximum depths of between 8.3 m and 9.7 m below ground level (bgl) at the locations illustrated in Figure 2. The resulting profiles of cone resistance q_c and friction ratio R_f are shown in Figure 3. The inferred soil profile comprises a layer of made ground/fill containing dense compacted gravel followed by stiff sandy clay to a maximum depth of ~ 1.8 m bgl, which in turn is underlain by medium dense to dense sand to a depth of ~ 6.5 m, below which the sand becomes increasingly gravelly. Variable values of q_c were noted in the made ground layer, before initially increasing with depth from ~ 10 MPa at 2 m bgl to ~ 20 MPa at 3.5 m bgl during penetration within the underlying sand. Cone resistances subsequently reduced again to minimum values of ~ 8 MPa at 4.5 m bgl, before becoming increasingly variable (q_c ~ 5 to 35 MPa) at depths in excess of 6.5 m bgl as the portion of gravel increased. Negligible pore pressures (< 10 kPa) were measured during penetration in all layers. A dissipation test was conducted at 7.0 m bgl during CPT01 to assess if the pore pressure response was a result of insufficient saturation of the piezocone; pore pressures remained

negligible during the 5 minute dissipation period, suggesting that the deposit is essentially unsaturated. While no additional groundwater monitoring was conducted, pumping test data obtained from an adjacent site revealed the water table to be present at a depth in excess of 15m bgl. The small-strain shear stiffness $G_{0,SCPT}$ of the soil was determined by performing a seismic cone penetration test (SCPT) in the centre of the test area, where a relatively constant $G_{0,SCPT}$ of ~ 110 MPa was evident within the sand stratum below a depth of 3.5 m (see Figure 3).

Samples retrieved from the test area at a depth of 3 m bgl revealed brown uniform fine to medium sand, with a mean effective particle size D_{50} of 0.3 mm, uniformity coefficient C_u of 1.69, specific gravity G_s = 2.65 ± 0.01, and minimum e_{min} and maximum void ratios e_{max} of 0.49 and 0.85 respectively. The sand particles can be described as sub-angular to sub-rounded (see Figure 4 for magnified images of the particles obtained using a Scanning Electron Microscope or SEM), with X-Ray Diffraction (XRD) analyses indicating quartz as the dominant mineral. The constant-volume friction angle φ'_{cv} of the sand was ~ 35°, based on a series of direct shear box tests conducted on air-pluviated sand samples at applied normal stresses varying from 40 kPa to 100 kPa. Further details of the laboratory tests are given in Flynn (2014).

PILE DETAILS AND EXPERIMENTAL PROGRAM

A total of three instrumented DCIS test piles, designated Piles R1, R2 and R3 respectively, were constructed, cured and load tested over a 28-day period during October and November 2013, the details of which are summarised in Table 1. The test piles had nominal shaft and base diameters of 320 mm and 380 mm respectively, with embedded lengths ranging from 5.5 m to 7.0 m. Each pile was reinforced over the full length using 4 no. 25 mm diameter steel bars, with shear reinforcement provided by an 8 mm diameter helical cage at 200 mm pitch. A schematic of the test piles is presented in Figure 5.

Instrumentation for each pile comprised 16 no. Geosense VW2100 vibrating-wire embedment strain gauges placed in arrays of four gauges at four separate levels (see Figure 5 for specific details) which were chosen to optimise measurements of local shear stress over a wide range of h/D_s values. The gauges were attached in a vertical orientation to steel rings welded to the inside the main reinforcement cage (see Figure 6). The uppermost set of gauges in each pile was deliberately placed at a distance of 2.0 m below the pile head to minimise the effects of localised non-uniform strains in the vicinity of the pile cap as highlighted by Lam and Jefferis (2011).

The test piles were constructed using a 320 mm outer diameter, 20 mm thick steel installation tube fitted with a 380 mm diameter sacrificial base plate which was driven to the required depth using a Junttan HHK5ASS hydraulic hammer. Upon completion of driving, the tube was filled with high-slump concrete with a 28-day characteristic strength of 35 N/mm^2 and subsequently extracted. The instrumented steel cage was inserted into the freshly-cast concrete after tube extraction in order to prevent damage to the strain gauge instrumentation. A concrete pile cap, with a nominal diameter of 450 mm, was constructed at the head of each test pile immediately after installation using a 700 mm deep steel casing embedded ~ 300 mm bgl.

The test piles were allowed to cure for a period of between 19 and 23 days (see Table 1) to enable the concrete to gain sufficient strength prior to performing the maintained compression load tests. Although a limited number of studies have reported the development of residual loads in cast-in-situ piles during curing, Flynn et al. (2012) concluded that the majority of these studies involved piles constructed in soft cohesive soils where consolidation-related settlements (and hence negative skin friction) was anticipated to occur. Furthermore, continuous monitoring of strain and temperature

behaviour during curing of the aforementioned Pile S1 in similar sand conditions at a site in north Wales (Flynn et al. 2013) revealed negligible residual loads during a 15 day curing period. Continuous monitoring of strain and temperature behaviour within the test piles at Ryton-on-Dunsmore during curing was therefore deemed unnecessary, but strain readings were taken immediately after casting and again prior to commencing each load test to ascertain the net change in strain with the test piles during this period.

Following the curing period, the test piles were subjected to maintained compression load tests in a consecutive manner, beginning with Pile R1. The load tests were performed by jacking the piles against a steel loading frame which was connected to 3 no. tension piles installed prior to the test piles. Four linear potentiometric displacement transducers (LPDT) rigidly mounted to an independent reference beam were used to measure the pile head displacements. Data acquisition during loading was obtained using a Campbell Scientific datalogger which was connected to the LPDTs, load cell and strain gauge instrumentation. The loading schedules typically entailed load increments equivalent to 10 % of the predicted pile capacity, with the magnitude of load increment reduced when pile failure was imminent. Each load increment was held constant until the pile settlement rate reduced to a minimum of 0.2 mm/hour, resulting in hold durations ranging from 30 minutes to 6 hours. Unload-reload cycles were omitted for ease of interpretation of strain within the test piles, based on experience from Pile S1 in north Wales (Flynn et al. 2013). The duration of the tests varied from ~ 24 hours for Pile R2 to ~ 60 hours for Pile R3.

RESULTS

Installation

The installation data for the three test piles, in terms of total blow count and number of blows per 250 mm penetration, are illustrated in Figure 7. The number of blows necessary to penetrate the made ground/fill layer between the surface and 1.8 m bgl was variable, ranging from ~ 30 blows for Pile R3 to ~ 105 blows for Pile R1 (see Figure 7a). However, similar sets were observed within the underlying sand layer for all piles, with the profiles of blows/250 mm tending to mirror the relevant CPT q_c profiles nearby (Figure 3).

Curing

The resulting distributions of net change in strain with depth after curing for the test piles are shown in Figure 8 where relatively uniform tensile strain profiles of ~ 65 με were evident for all three piles. Such observations are in keeping with the tensile strain profiles measured after curing of instrumented DCIS piles in similar ground conditions by Flynn et al. (2013) and Flynn (2014), and are primarily due to restraint of the pile during the process of drying shrinkage (Kim et al. 2011; Sinnreich 2012). Furthermore, the relatively uniform distribution of tensile strains with depth are in contrast with similar studies of cast-in-situ piles in clay (Fellenius et al. 2009; Flynn et al. 2012; Kim et al. 2011), whereby large compressive strains developed within the lower sections of the piles due to residual loads resulting from consolidation-related settlement of the soft cohesive layers in which the piles were installed. It is therefore concluded that negligible residual loads were present in the test piles after curing.

Load testing

Figure 9 shows the measured load-displacement response of the three test piles during maintained compression loading. A near-identical load-displacement response was evident for all piles during the initial stages of loading, with significant creep displacements evident for Piles R1 and R2 at applied loads in excess of 1400 kN. Creep displacements were considerably less for Pile R3, despite the fact that Piles R2 and R3 were constructed using the same concrete mix. Pile head displacements increased significantly during the latter stages of loading of Piles R1 and R2, resulting in total pile resistances at pile head displacements equivalent to 10 % of the pile base diameter $Q_{t,0.1Db}$ of 1620 kN and 1580 kN respectively. Pile R3, on the other hand, continued to exhibit a stiff response in comparison to the other piles at applied loads greater than 1400 kN, with the test eventually being terminated when the maximum safe working load of the loading frame was reached. Hyperbolic extrapolation of the load-displacement curve to a displacement of 38 mm (i.e. $0.1D_b$) using the method by Chin (1972) resulted in an estimated total pile resistance of 2280 kN. Given the similarity in ground conditions (as evident from the CPT profiles) and installation data at the test location, the significantly greater resistance of Pile R3 in comparison to Piles R1 and R2 was somewhat unexpected and was subsequently investigated further during analysis of shaft and base resistance.

The strain gauge instrumentation enabled the total resistance to be separated into the respective shaft and base components. The strain data at the uppermost gauge level (i.e. 2.0 m bgl) were used to derive the relationship between the pile stiffness E_p and applied strain level for each pile using the secant modulus method (Lam and Jefferis 2011). Creep-related strain effects were also accounted for using the method described by Lam and Jefferis (2011). Further details regarding the strain interpretation process are described by Flynn (2014).

Base resistance

While this paper is primarily concerned with the shaft resistance of DCIS piles in sand, it is important to assess the contribution of the base resistance to the total resistance of the test piles. Figure 10 shows the base stress-displacement response of the three test piles during loading. A stiff linear manner was evident for all piles during the initial stages of loading, with the base-displacement curves for Piles R1 and R2 essentially identical. However, Pile R3 mobilised a greater base resistance for a given displacement in comparison to Piles R1 and R2 during the latter stages of loading. It was therefore concluded that the greater total resistance observed for Pile R3 in comparison to Piles R1 and R2 was a consequence of the significantly larger base resistance of the pile during loading.

Shaft resistance

Average shear stresses

The variation in average shear stress $\tau_{s,avg}$ (=shaft resistance/shaft area) mobilised along the shaft of each pile during loading within the sand layer below 2.0 m bgl is shown in Figure 11. A ductile shaft resistance response was evident for the test piles, with shaft displacements in excess of 15 mm required to mobilise peak values. Such displacements, which correspond to normalised values w_s/D_s of ~ 4 %, are significantly greater than those reported for traditional displacement piles (typically equivalent to 2% of the pile diameter according to Fleming et al., 2007), but broadly in line with displacements observed by Gavin et al. (2009) for two instrumented CFA piles (with nominal diameters of 450 mm and 600 mm respectively) during maintained compression load testing in sand.

Local shear stresses

The local shear stresses $\tau_{s,loc}$ on the pile shafts were derived assuming a linear reduction in load between each gauge level. Figure 12 shows the mobilisation of $\tau_{s,loc}$ with local shaft displacement w_s (i.e. accounting for elastic pile compression) during loading of Piles R1, R2 and R3. In a similar manner to the average shear stress profiles, large local shaft displacements were typically necessary to mobilise peak values. The distribution of local shear stress at failure (defined as the peak value of $\tau_{s,loc}$) with depth for the test piles is shown in Figure 13. The profiles tend to mirror the nearest CPT q_c profile shown in Figure 3, with lower local shear stresses mobilised between 3.5 m and 5 m bgl where reductions in q_c were apparent (~ 10 MPa) in comparison to the upper and lower sections of the sand layer (q_c ~ 15 MPa). Furthermore, the largest peak local shear stresses were mobilised at sections closest to the base of each test pile. The variation in local shear stresses, normalised by the corresponding average cone resistance q_c between gauge levels, with normalised distance from the pile base h/D_s is illustrated in Figure 14. In keeping with the behaviour of closed-ended displacement pile during installation and loading in sand reported by Lehane et al. (1993), Chow (1997) and others, a general trend of τ_{sf}/q_c reducing with increasing h/D_s is evident for the three test piles, suggesting that friction fatigue is a key mechanism governing the shaft resistance of DCIS piles in sand.

DISCUSSION

In this section, the shaft resistance of the instrumented DCIS piles during loading is examined in more detail and subsequently compared with the studies of preformed displacement piles in sand discussed previously. Firstly, it is of interest to compare the values of lateral earth pressure at failure K_f, back-figured from the measured local shear stresses at failure τ_{sf} for the test piles using Equation 1. As shown in Figure 15, the K_f values inferred from the measured local shear stresses are significantly greater than K_f = 1.0 (Fleming et al. 2007). As a result, the recommendations by Fleming et al. (2007) would have significantly under-estimated the shaft resistance of the test piles.

The average shear stress $\tau_{s,avg,}$ mobilisation curves, presented previously in Figure 11, were normalised by the corresponding average cone resistance $q_{c,avg}$ along the shaft of each pile in the sand layer (i.e. at depths in excess of 2.0 m bgl). The resulting curves of normalised average shear stress are shown in Figure 16, where peak values of $\tau_{s,avg}/q_{c,avg}$ ranged between 0.009 and 0.013. These values are greater than the typical range for closed-ended steel displacement piles reported by Gavin and Lehane (2003), primarily due to the increased interface friction angle of the DCIS piles resulting from the rougher shaft interface created by in-situ casting of the concrete; this results in shearing occurring within the sand mass adjacent to the pile shaft (i.e. $\delta_{cv} = \phi'_{cv}$) and not at the pile-soil interface as is the case with steel piles. Also shown in Figure 16 is the normalised average shear stress observed during maintained compression loading of Pile S1 in north Wales (Flynn et al. 2013). The mobilisation of $\tau_{s,avg}/q_{c,avg}$ is near-identical to the three test piles during the initial stages of loading, although an unload-reload cycle performed during the test led to a reduction in average shear stress (in keeping with the friction fatigue effects described previously). Consequently, Pile S1 mobilised a peak $\tau_{s,avg}/q_{c,avg}$ of ~ 0.01 at the end of the load test.

The large displacements necessary to achieve peak average and local shear stresses during loading for the three test piles are in stark contrast to the stiff compressive shaft resistance response typically observed for traditional preformed displacement piles, as highlighted previously. It is likely that the increased shaft roughness created by in-situ concreting plays a dominant role in the ductile response in shaft resistance during loading, particularly given the similar behaviour reported for CFA piles in sand by Gavin et al. (2013). Furthermore, the absence of driving-related residual stresses (due to the extraction of the steel installation tube after concreting) may also give rise to a softer shear stress response during compressive loading, as demonstrated by Alawneh (2005). The influence of stress relief during tube extraction is also plausible, although the large peak shear stresses generated during loading suggest such an effect is subsequently recoverable.

As outlined previously, the variations in radial stress on the shafts of the test piles during loading were not measured directly due to lack of instrumentation capable of withstanding the in-situ concreting process. However, the local radial effective stresses at failure σ'_{rf} were inferred from the measured peak local shear stresses using Equation 2, assuming δ_{cv} is equivalent to the constant-volume friction angle ϕ'_{cv} of the sand. The resulting variation in σ'_{rf} with depth for the three test piles is shown in Figure 17, together with the idealised distribution of radial stress imposed on the surrounding soil by the head of concrete after casting and tube extraction (assuming a unit weight of concrete γ_c of 24 kN/m^3). The inferred values of σ'_{rf}, ranging from ~ 140 kPa to ~ 290 kPa, are significantly greater than the postulated radial stresses exerted on the surrounding soil by the head of concrete after extraction of the installation tube, thus demonstrating that the large radial stresses generated by displacement of the soil during driven installation of the steel tube were not erased upon concreting and tube withdrawal. It is plausible that suction pressures within the unsaturated sand may have prevented relaxation of the displaced soil during tube removal. However, the radial stresses are broadly in line with those inferred by Flynn et al. (2013) for Pile S1 at Shotton which was constructed in saturated sand.

In a similar manner to Figure 14, the radial effective stresses at failure inferred from the measured local shear stresses for the three instrumented tests were normalised by the corresponding average cone resistance q_c between gauge levels and plotted against normalised distance from the pile base h/D_s in Figure 18. A regression analysis performed on the dataset for the three test piles led to the following equation for estimating the reduction in σ'_{rf} with increasing distance from the pile base:

$$\sigma'_{rf} = 0.031 q_c \left(\frac{h}{D_s} \right)^{-0.41} \qquad \text{Eqn. 5}$$

The similarity between Equation 5 and the normalised stationary radial stress (i.e. no dilation) after installation σ'_{rc}/q_c proposed by the UWA-05 method (Lehane et al. 2005) for driven preformed displacement piles in Equation 3 is immediately apparent. This provides further validation of the applicability of the UWA-05 pile design method in estimating the capacity of temporary-cased DCIS piles in sand (as demonstrated by Flynn et al., 2014). The comparison between Equations 3 and 5 is further illustrated in Figure 18; values of σ'_{rf}/q_c inferred from the measured local shear stresses are slightly under-estimated by Equation 3, suggesting that modest increases in radial stress (due to interface dilation) may have occurred during loading of the test piles. Unfortunately, the lack of suitable radial stress instrumentation for cast-in-situ pile types prevents confirmation of this phenomenon.

CONCLUSIONS

A series of maintained compression load tests were performed on three temporary-cased DCIS piles constructed in a uniform sand deposit, with instrumentation enabling the shaft and base resistances of the piles to be accurately measured during loading. The following conclusions regarding the shaft resistance of temporary-cased DCIS piles in sand have been reached:

1. The shaft displacements necessary to mobilise peak local and average shear stresses were in excess of those typically reported for preformed displacement piles and more comparable with those observed for replacement cast-in-situ pile types.
2. Coefficients of lateral earth pressure at failure K_f back-figured from the measured local shear stresses were significantly greater than K_f = 1.0 recommended by Fleming et al. (2007) for design of DCIS piles in sand.
3. A ductile shaft resistance response was evident during loading of the three DCIS piles. Such behaviour, which is in stark contrast to the stiff behaviour of traditional preformed displacement piles during compressive loading, was attributed to the increased interface

friction angle created by the rougher shaft interface of the piles, as well as the absence of driving-related residual stresses due to extraction of the installation tube after concreting.

4. A reduction in normalised local shear stresses $\tau_{s,loc}/q_c$ and normalised radial effective stresses at failure σ'_{rf}/q_c with increasing normalised distance from the pile base h/D_s was evident for the instrumented DCIS test piles. This phenomenon, known as friction fatigue, is a well-known characteristic of preformed displacement piles and its existence for DCIS piles implies that radial stresses induced during driven installation of the steel tube are not erased upon concreting of the pile/withdrawal of the tube.
5. The inferred normalised radial stresses at failure showed good agreement with the idealised σ'_{rf}/q_c profile for traditional preformed closed-ended displacement piles predicted by the UWA-05 CPT-based design method and therefore provides further validation for the use of this design method for estimating the shaft resistance of temporary-cased DCIS piles in sand.

ACKNOWLEDGEMENTS

The authors wish to acknowledge Keller Foundations UK for sponsoring the test programme and constructing the piles, and to Dr. Derek Egan in particular for his support throughout. The authors would also like to thank Darren Ward and InSitu Site Investigation Ltd. for performing the CPTs, Edward Meade and NVM Ltd. Ireland for supplying the strain gauge instrumentation and Environmental Scientifics Group (ESG) Ltd. for performing the load tests and strain gauge data acquisition. The authors also wish to thank Alan Duggan and the Department of Chemistry, NUI Galway for performing the mineralogy and magnification tests. The financial assistance provided to the first author by the College of Engineering & Informatics Research Fellowship and University Foundation Bursary is also gratefully acknowledged.

REFERENCES

Alawneh, A.S. 2005. Modelling load-displacement response of driven piles in cohesionless soils under tensile loading. Computers and Geotechnics, **32**(8): 578–586.

Boulon, M., and Foray, P. 1986. Physical and numerical simulation of lateral shaft friction along offshore piles in sand. *In* Proceedings of the 3rd International Conference on Numerical Methods in Offshore Piling, Paris, France, pp. 127–148.

Briaud, J.-L., and Tucker, L.M. 1988. Measured and predicted axial response of 98 piles. Journal of Geotechnical Engineering, **114**(9): 984–1001.

British Standards Institute (BSI). 1986. BS 8004 - Code of Practice for Foundations. British Standards Institution, London, United Kingdom.

Chin, F. 1972. The inverse slope as a prediction of ultimate bearing capacity of piles. *In* Proceedings of the 3rd South-East Asian Conference on Soil Engineering, pp. 83–91.

Chow, F.C. 1997. Investigations into the behaviour of displacement piles for offshore foundations. Ph.D. thesis, University of London (Imperial College), London, United Kingdom.

Fellenius, B.H., Kim, S.R. and Chung, S.G. 2009. Long-term monitoring of strain in instrumented piles. Journal of Geotechnical and Geoenvironmental Engineering, **135**(11): 1583–1595.

Fleming, W.G.K., Weltman, A., Elson, K. and Randolph, M.F. 2008. Piling Engineering. 3rd Edition. Taylor & Francis, London, United Kingdom.

Flynn, K.N. 2014. Experimental investigations of driven cast-in-situ piles. Ph.D. thesis, College of Engineering & Informatics, National University of Ireland, Galway, Ireland.

Flynn, K.N., McCabe, B.A. and Egan, D. 2012. Residual load development in cast-in-situ piles – a review and new case history. *In* Proceedings of the 9th International Conference on Testing and Design Methods for Deep Foundations (IS Kanazawa), 18-20 September 2012, Kanazawa, Japan, pp. 765–773.

Flynn, K.N., McCabe, B.A. and Egan, D. 2013. The axial load behavior of a driven cast-in-situ pile in sand. *In* Proceedings of the 7th International Conference on Case Histories in Geotechnical Engineering, 1-4 May 2013, Chicago, USA, pp. 1–6.

Flynn, K.N., McCabe, B.A. and Egan, D. 2014. Driven cast-in-situ piles in granular soil: applicability of CPT methods for pile capacity. *In* Proceedings of the 3rd International Symposium on Cone Penetration Testing (CPT'14), 12-14 May 2014, Las Vegas, USA, pp.1–8.

Gavin, K.G., and Lehane, B.M. 2003. The shaft capacity of pipe piles in sand. Canadian Geotechnical Journal, **45**(1): 36–45.

Gavin, K.G., and O'Kelly, B.C. 2007. Effect of friction fatigue on pile capacity in dense sand. Journal of Geotechnical and Geoenvironmental Engineering, **133**(1): 63–72.

Gavin, K.G., Cadogan, D. and Casey, P. 2009. Shaft capacity of continuous flight auger piles in sand. Journal of Geotechnical and Geoenvironmental Engineering, **135**(6): 790–798.

Heerema, E.P. 1980. Predicting pile driveability: Heather as an illustration of the "friction fatigue" theory. Ground Engineering, **13**(4): 15–20.

Jardine, R.J., Chow, F.C., Standing, J.R., Overy, R.F., Saldivar, E.E., Strick van Linschoten, C. and Ridgway, A. 2005. An updated assessment of the ICP pile capacity procedures. *In* Proceedings of the 1st International Conference on Frontiers in Offshore Geotechnics, Perth, Australia, pp. 691–696.

Kim, S.R., Chung, S.G. and Fellenius, B.H. 2011. Distribution of residual load and true shaft resistance for a driven instrumented test pile. Canadian Geotechnical Journal, **48**(4): 583–598.

Lam, C., and Jefferis, S.A. 2011. Critical assessment of pile modulus determination methods. Canadian Geotechnical Journal, **48**(10): 1433–1448.

Lehane, B.M. 1992. Experimental investigations of pile behaviour using instrumented field piles. Ph.D. thesis, University of London (Imperial College), London, United Kingdom.

Lehane, B.M., and Jardine, R.J. 1994. Shaft capacity of driven piles in sand: a new design method. *In* Proceedings of the 7th International Conference on the Behaviour of Offshore Structures, Boston, Massechussetts, USA, Vol. 1, pp. 23–36.

Lehane, B.M., and White, D.J. 2005. Lateral stress changes and shaft friction for model displacement piles in sand. Canadian Geotechnical Journal, **42**(4): 1039–1052.

Lehane, B.M., Jardine, R.J., Bond, A.J. and Frank, R. 1993. Mechanisms of shaft friction in sand from instrumented pile tests. Journal of Geotechnical Engineering, **119**(1): 19–35.

Lehane, B.M., Gaudin, C. and Schneider, J.A. 2005a. Scale effects on tension capacity for rough piles buried in dense sand. Géotechnique, **55**(10): 709–719.

Lehane, B.M., Schneider, J.A. and Xu, X. 2005b. The UWA-05 method for predction of axial capacity of driven piles in sand. *In* Proceedings of the 1st International Conference on Frontiers in Offshore Geotechnics, Perth, Australia, pp. 683–689.

Randolph, M.F. 2003. Science and empiricism in pile foundation design. Géotechnique, **53**(10): 847–875.

Randolph, M.F., Dolwin, J. and Beck, R. 1994. Design of driven piles in sand. Géotechnique, **44**(3): 427–448.

Schneider, J.A., Xu, X. and Lehane, B.M. 2008. Database assessment of CPT-based design methods for axial capacity of driven piles in siliceous sands. Journal of Geotechnical and Geoenvironmental Engineering, **134**(9): 1227–1244.

Sinnreich, J. 2012. Strain gage analysis for nonlinear pile stiffness. Geotechnical Testing Journal, **35**(2): 1–7.

Shotton, F.W. 1953. The Pleistocene deposits of the area betwen Coventry, Rugby and Leamington and their bearing upon the topographic development of the Midlands. Philosophical Transactions of the Royal Society of London - Series B, Biological Sciences. **237**(646): 209–260.

Tomlinson, M., and Woodward, J. 2008. Pile Design and Construction Practice. 5th Edition. Taylor & Francis, London, United Kingdom.

Toolan, F.E., Lings, M.L. and Mirza, U.A. 1990. *In* Proceedings of the 22nd Offshore Technology Conference (OTC 6422), 7-10 May, 1990, Houston, Texas, pp.33–42.

White, D.J., and Lehane, B.M. 2004. Friction fatigue on displacement piles in sand. Géotechnique, **54**(10): 645–658.

Table 1. Details of test piles

Pile Ref.	Shaft diameter D_s (mm)	Base diameter D_b (mm)	Length L (m)	Installation date	Static load test date
R1	320	380	6.0	10th October 2013	30th October 2013
R2	320	380	7.0	11th October 2013	1st November 2013
R3	320	380	5.5	11th October 2013	4th November 2013

Table 1. Details of test piles

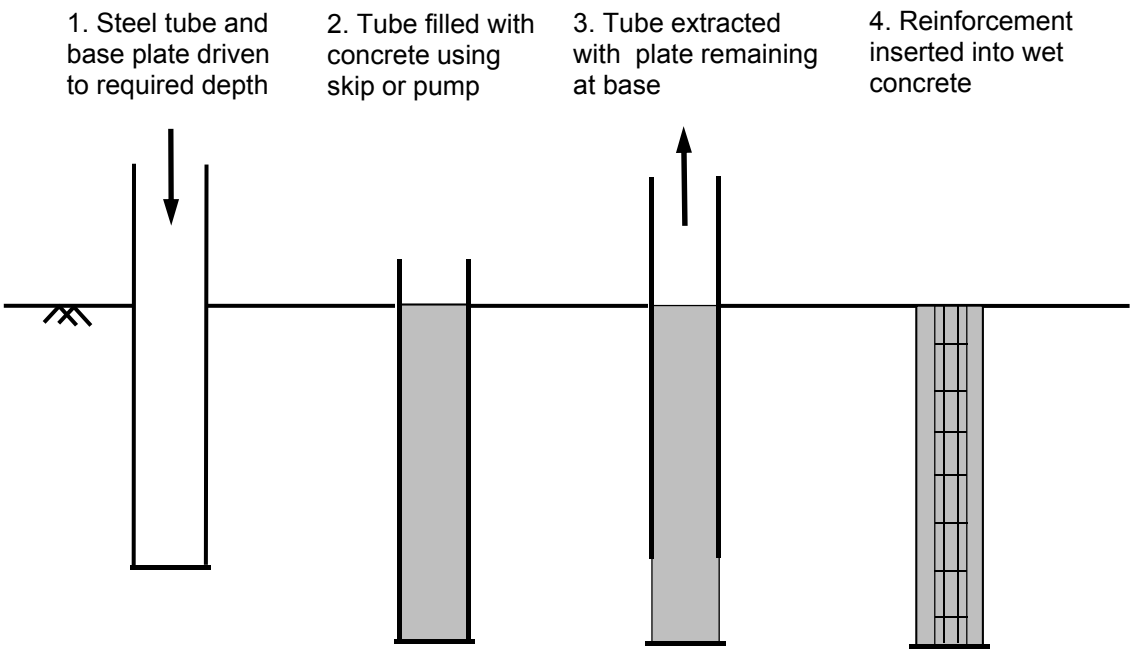

Fig. 1. Driven cast-in-situ pile construction sequence.

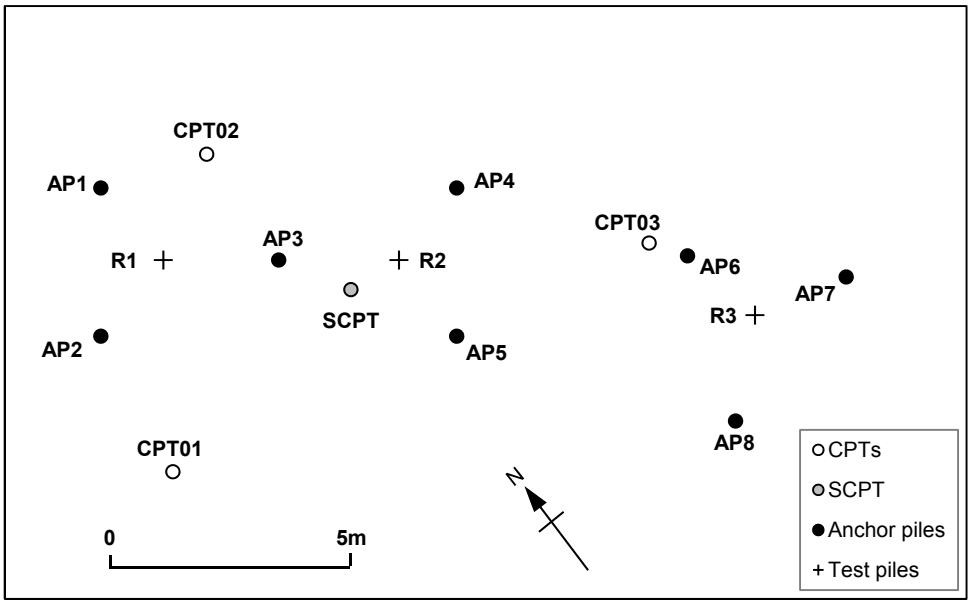

Fig 2. Layout of test piles and in-situ tests.

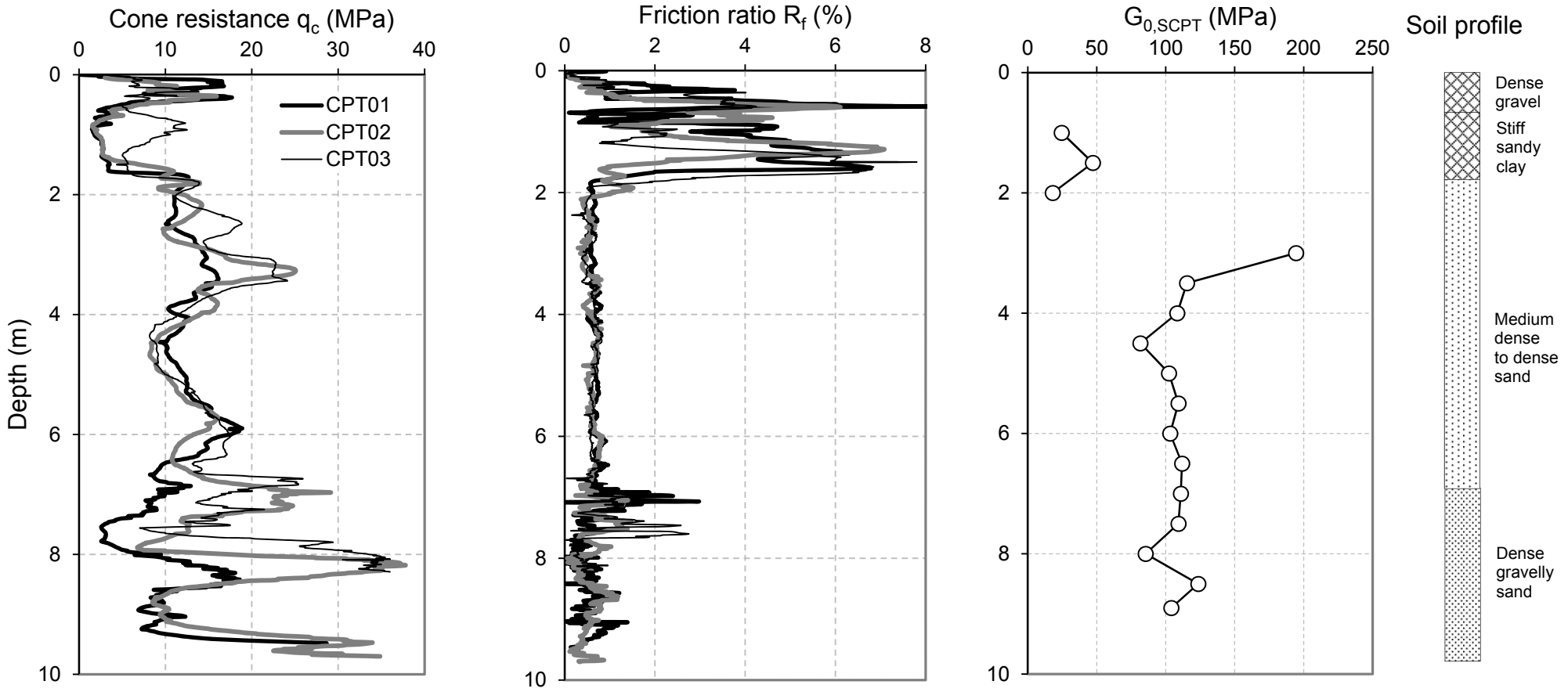

Fig. 3. CPT results.

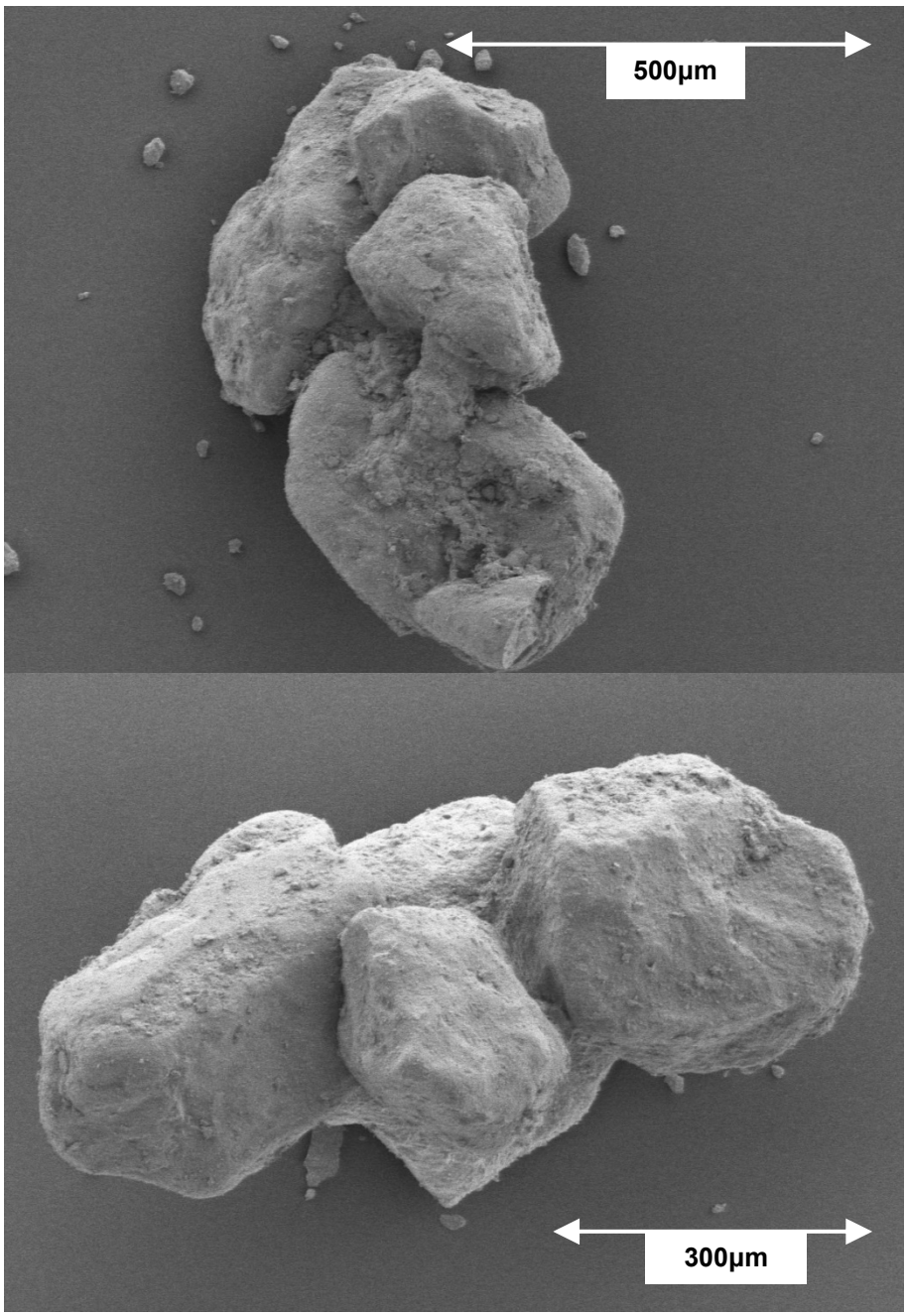

Fig. 4. Magnified images of sand particles.

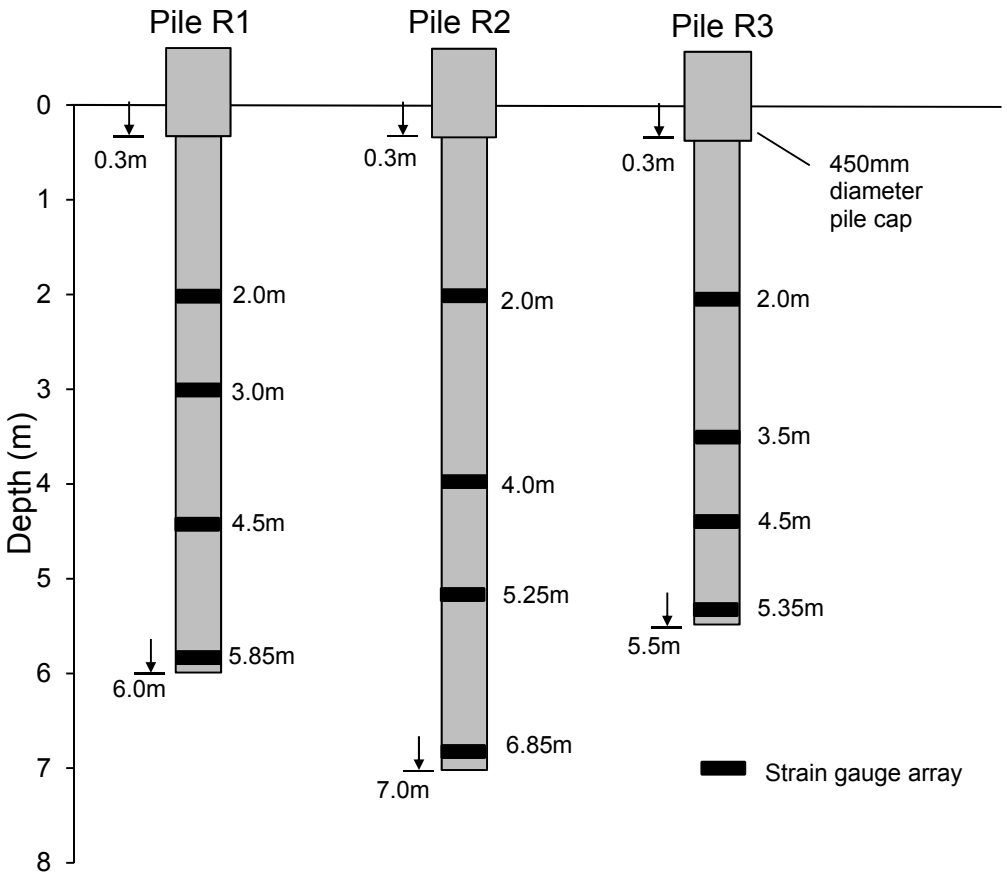

Fig. 5. Test pile details.

Fig. 6. Arrangement of vibrating wire strain gauge array.

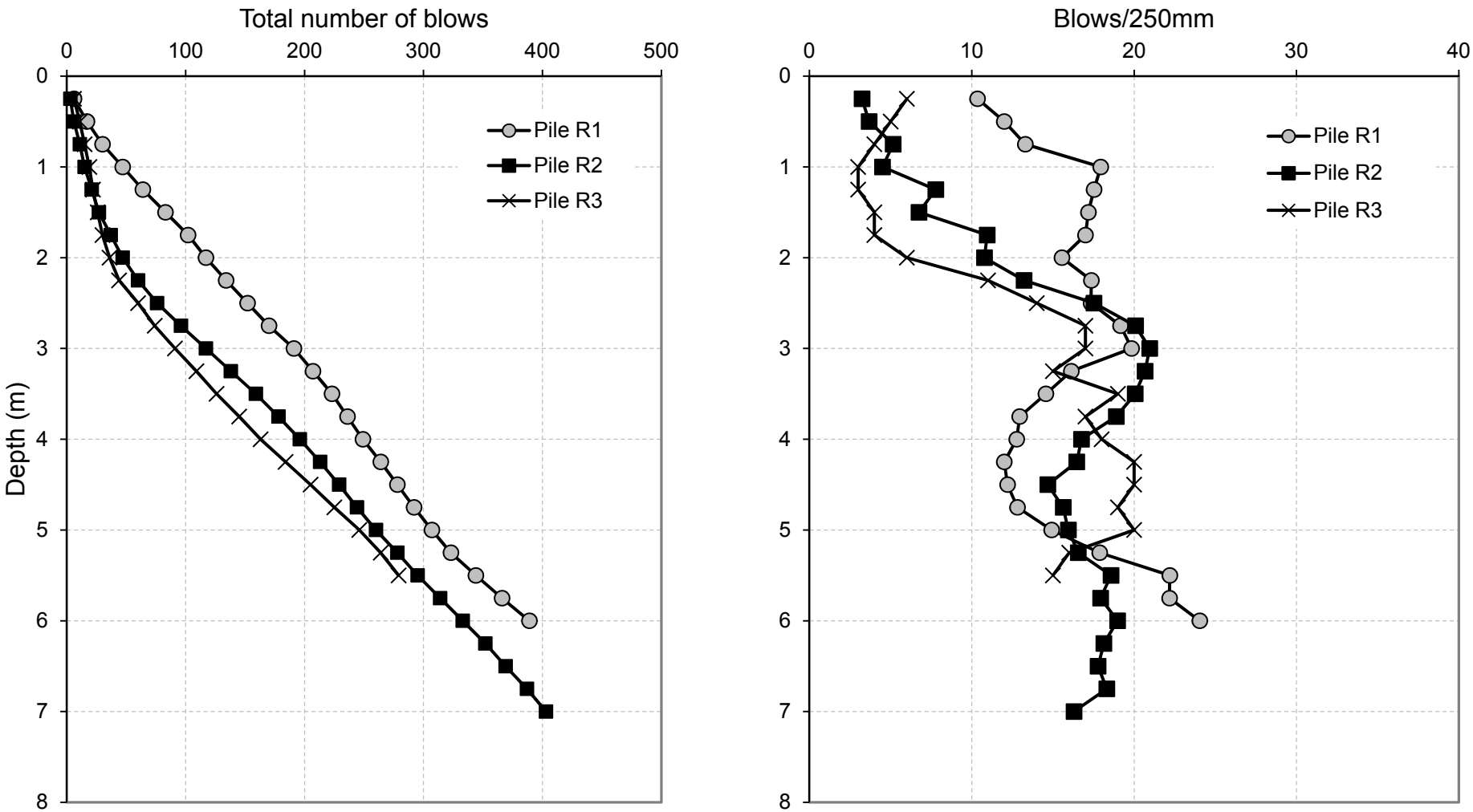

Fig. 7. *(a)* Total number of blows and *(b)* blows/250 mm during installation.

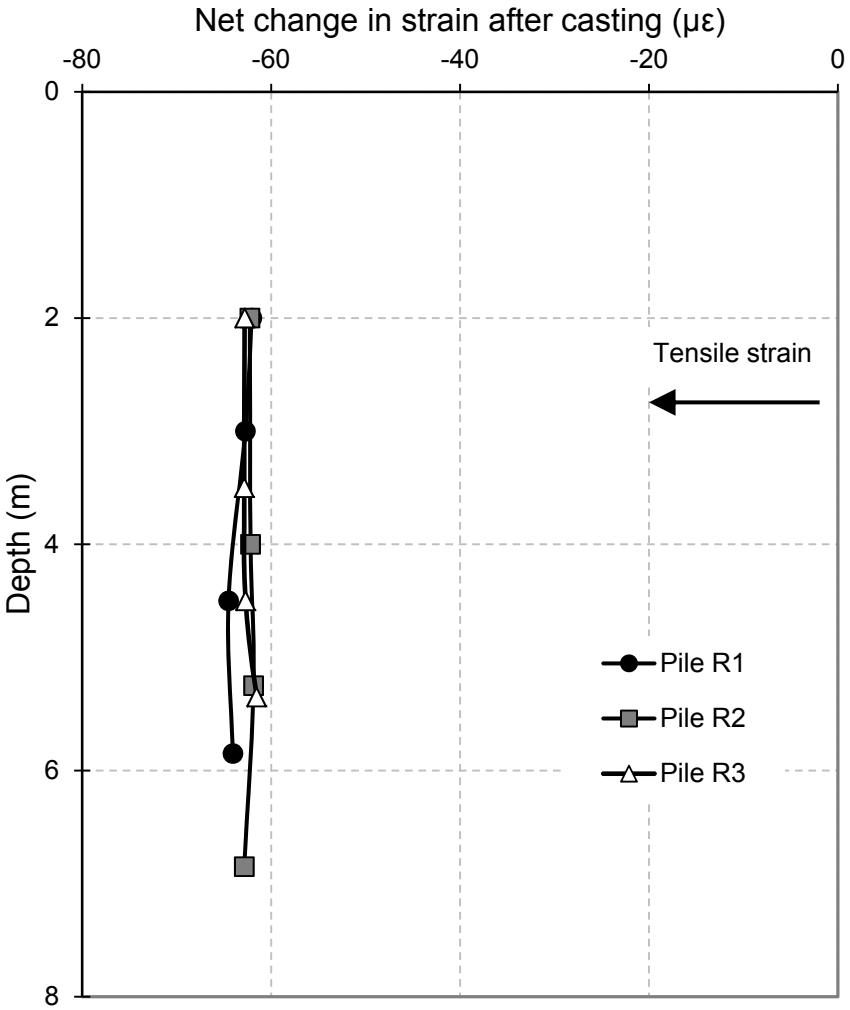

Fig. 8. Net change in strain after curing.

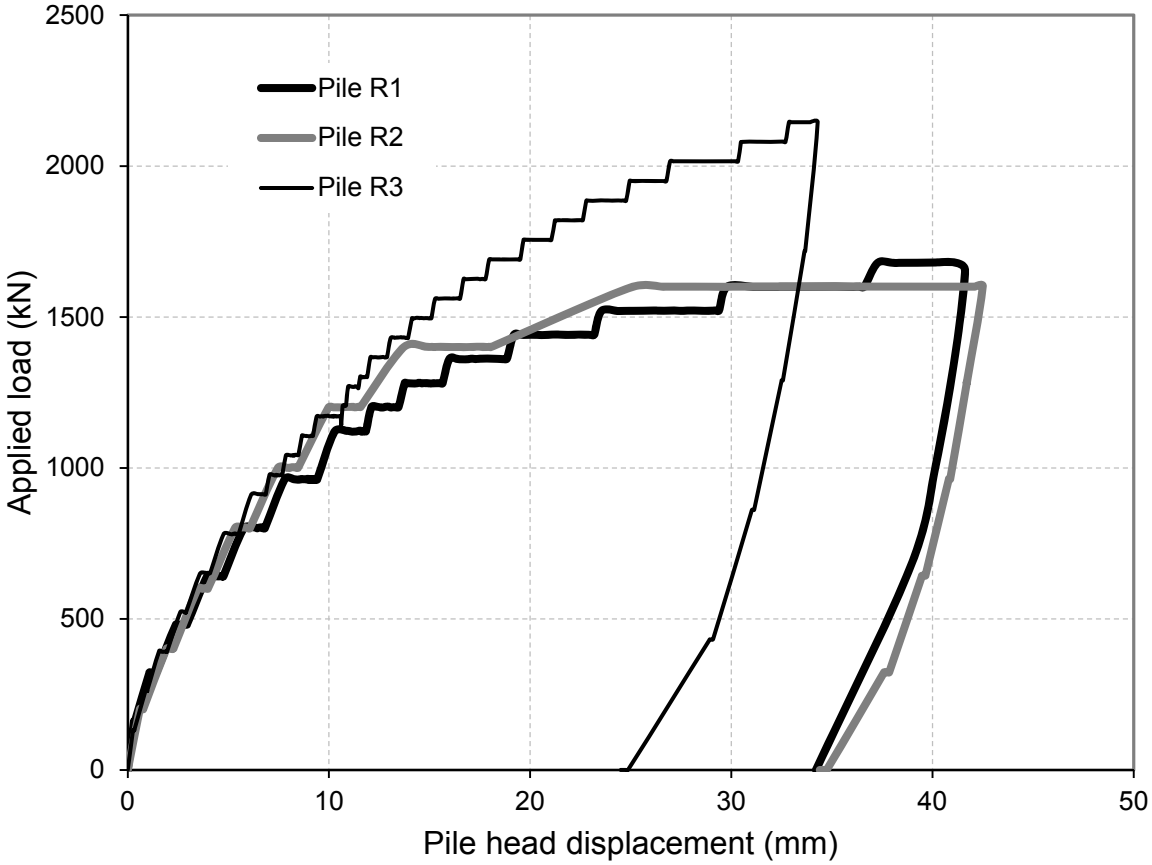

Fig. 9. Load-displacement response.

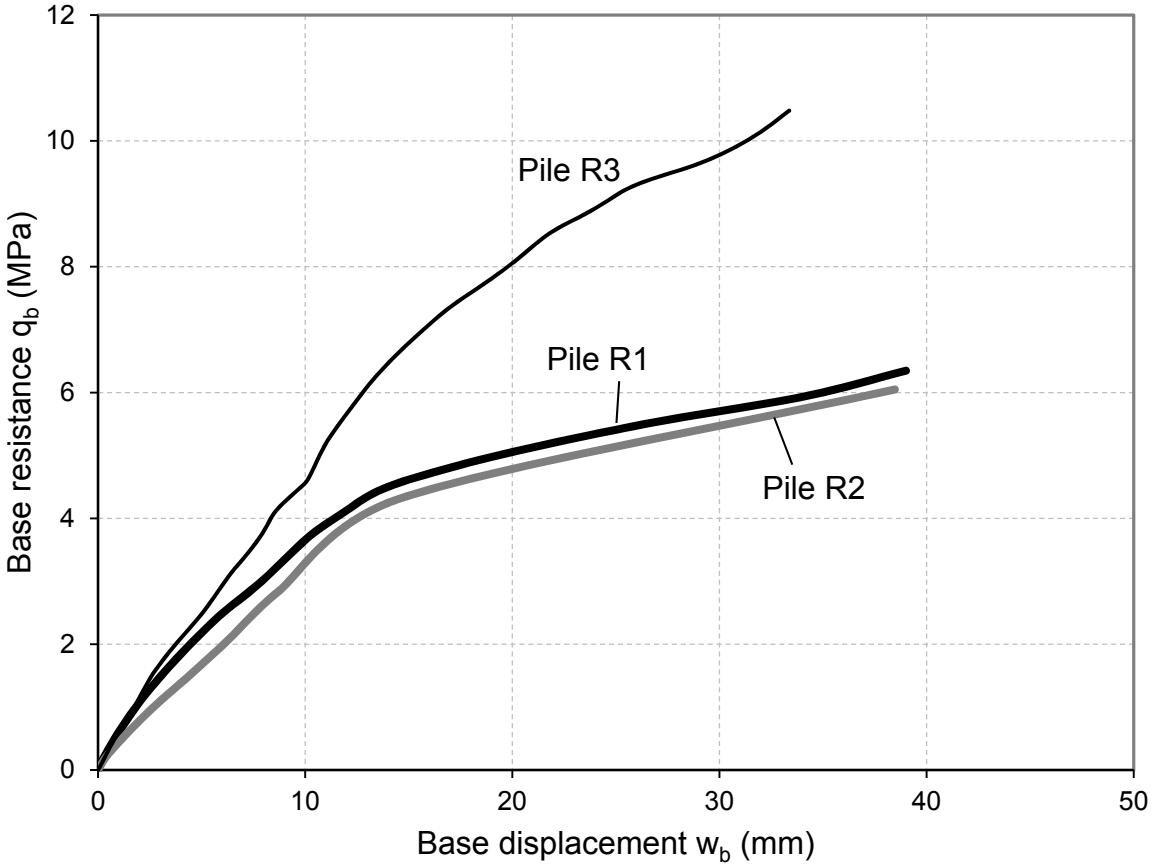

Fig. 10. Base resistance-displacement response.

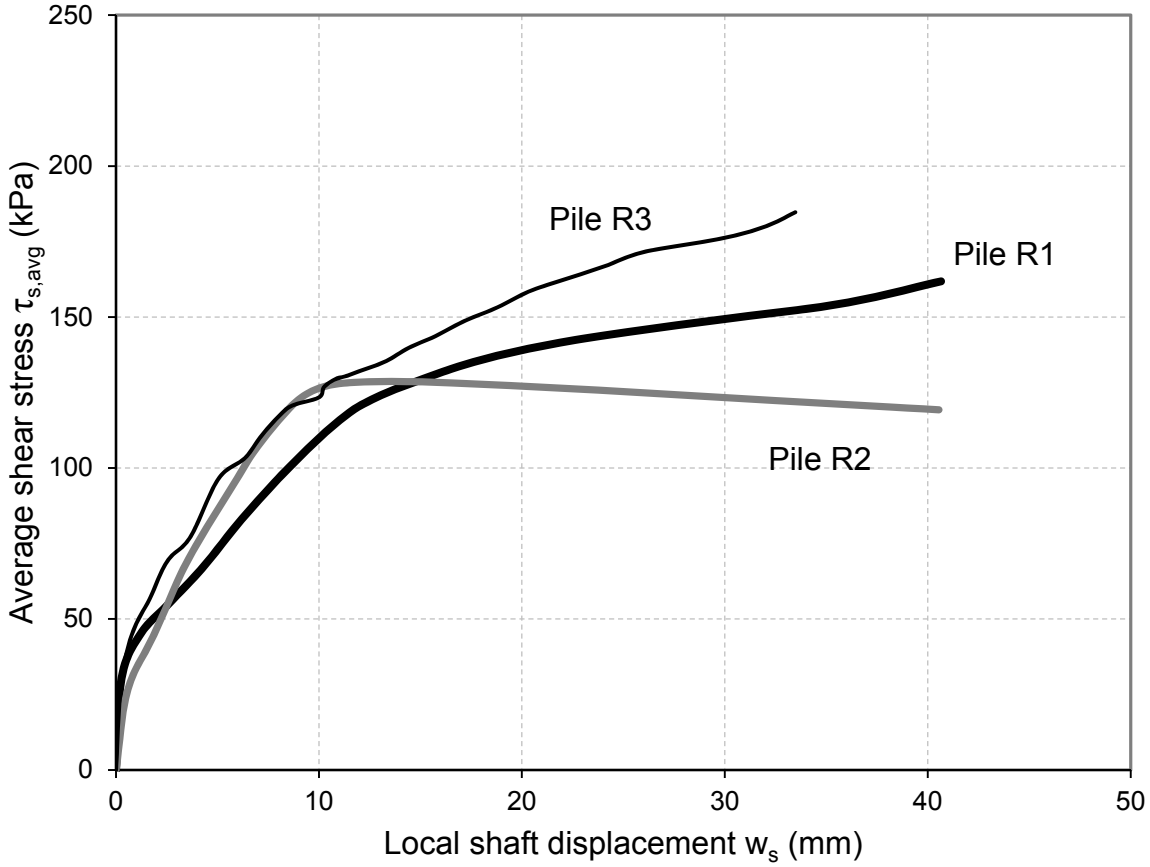

Fig. 11. Average shear stress mobilisation during loading.

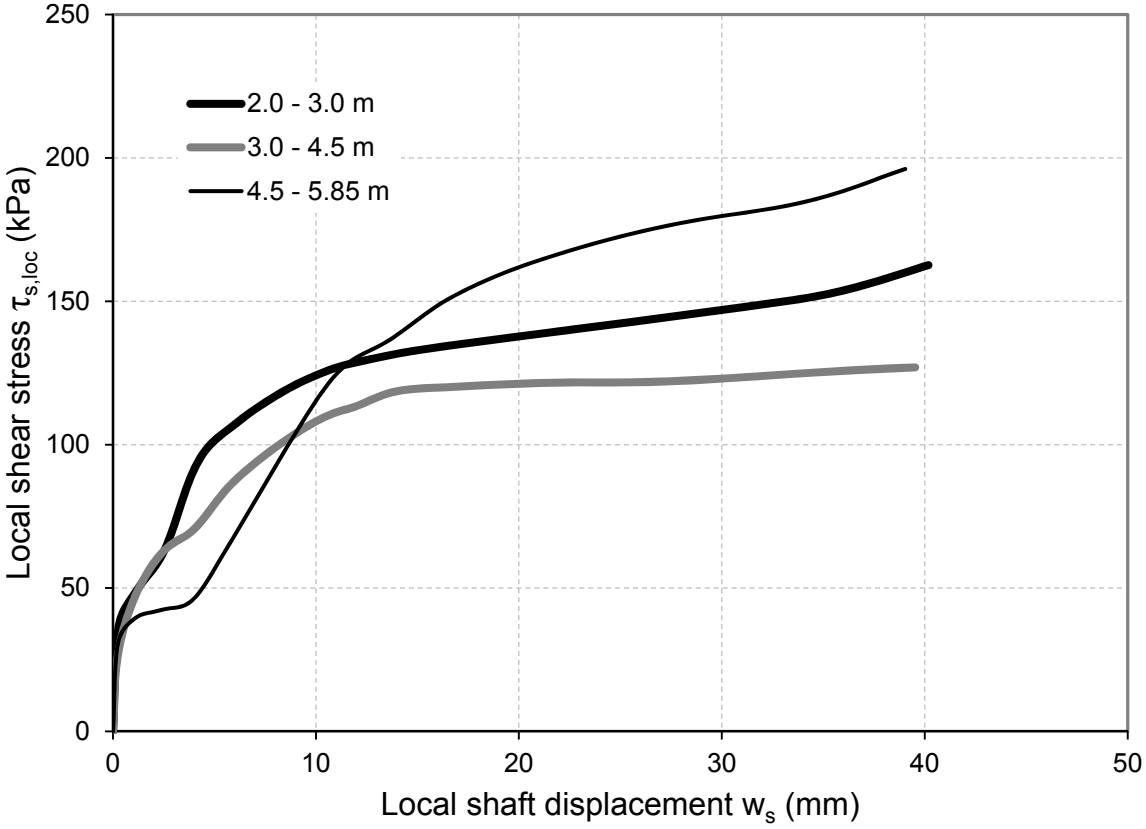
2.0 - 3.0 m
3.0 - 4.5 m
4.5 - 5.85 m
Local shear stress $\tau_{s,loc}$ (kPa)
Local shaft displacement w_s (mm)
0
50
100
150
200
250
0
10
20
30
40
50

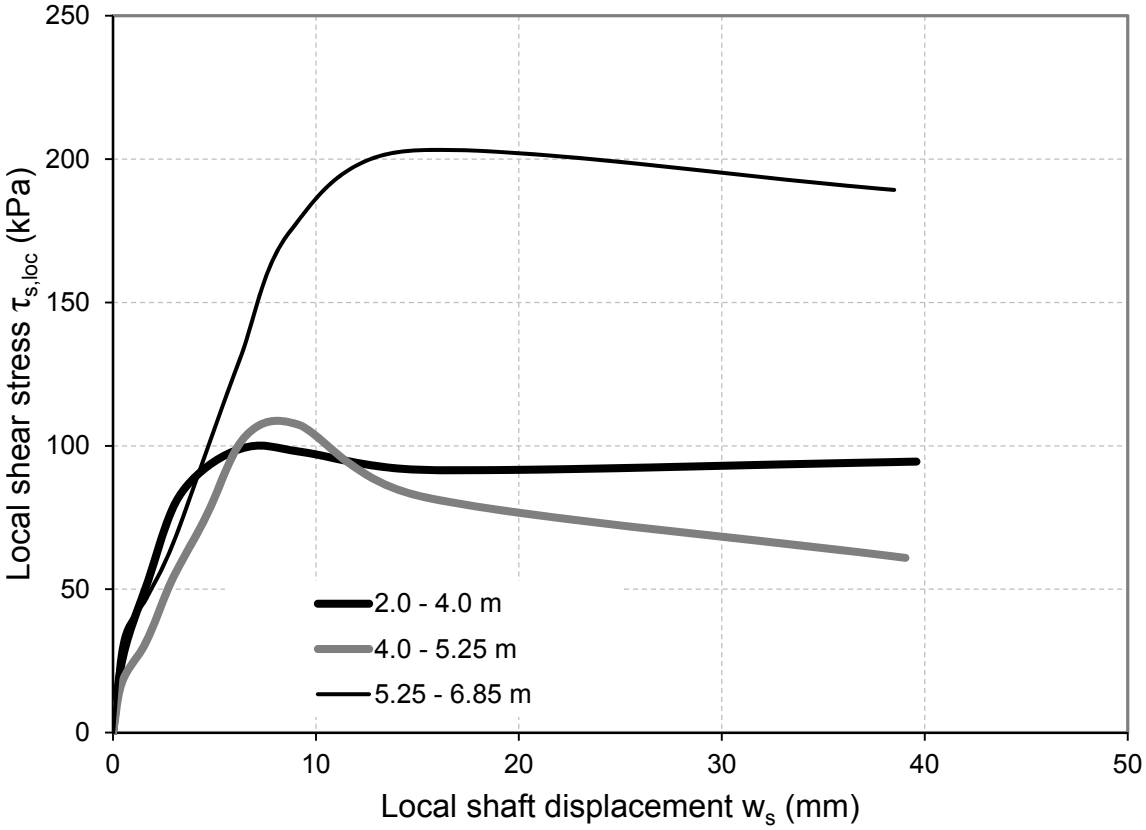
2.0 - 4.0 m
4.0 - 5.25 m
5.25 - 6.85 m
Local shear stress $\tau_{s,loc}$ (kPa)
Local shaft displacement w_s (mm)
0
50
100
150
200
250
0
10
20
30
40
50

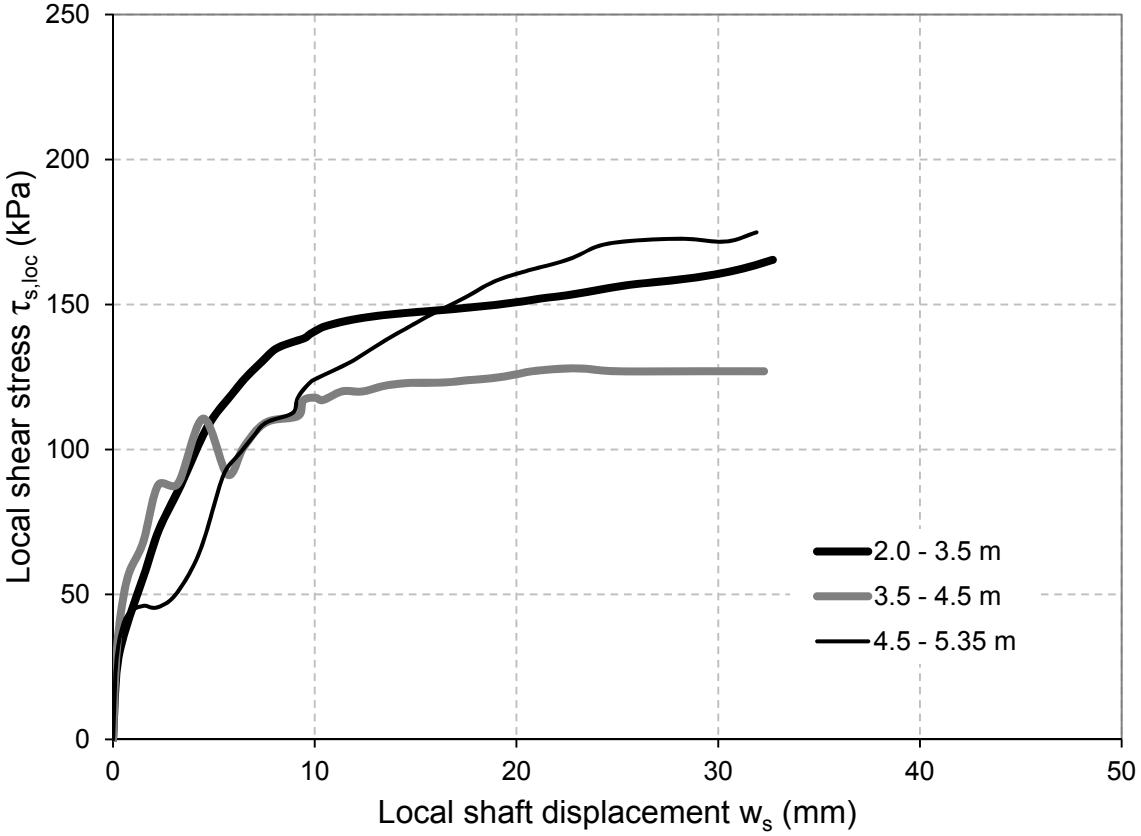

Fig. 12. Variation in local shear stresses with local shaft displacement during loading for *(a)* Pile R1, *(b)* Pile R2 and *(c)* Pile R3.

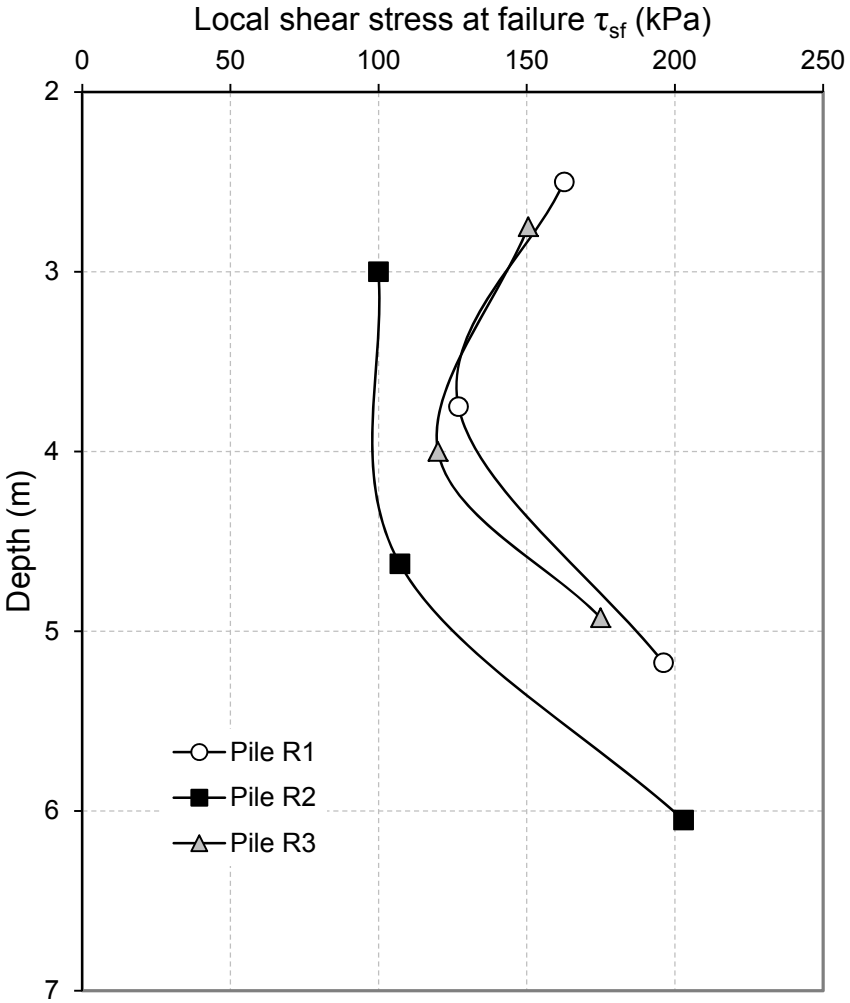

Fig. 13. Variation in local shear stresses at failure with depth.

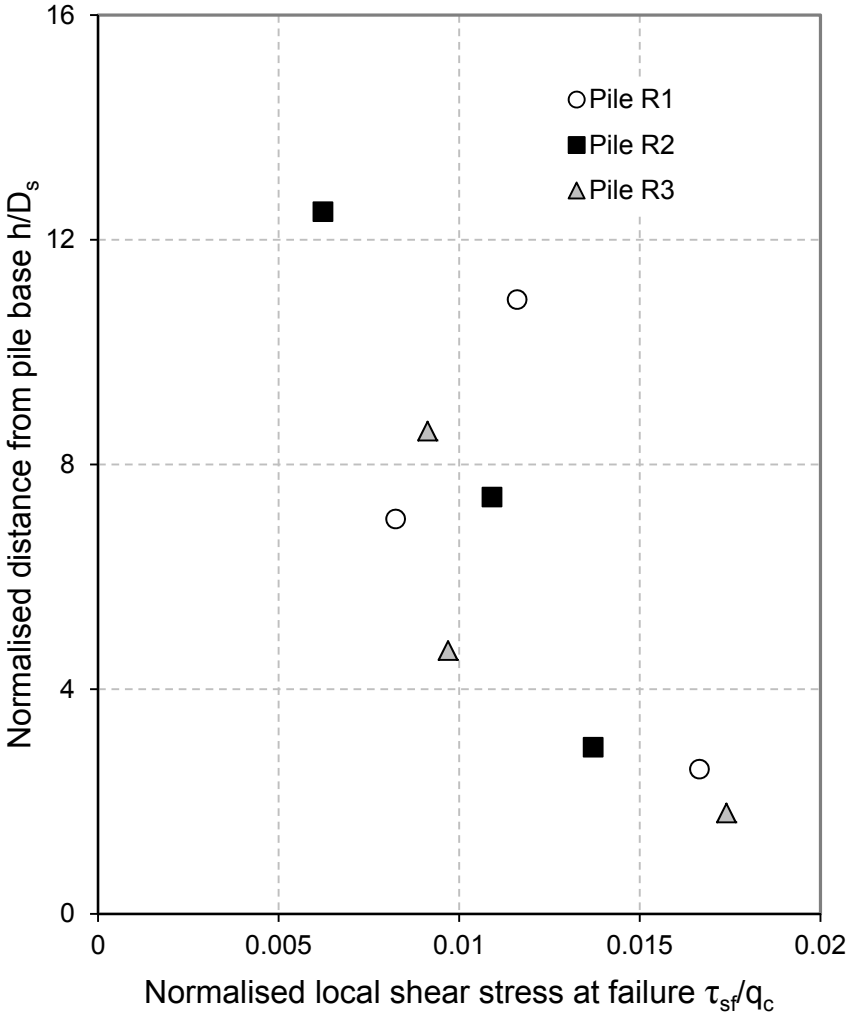

Fig. 14. Reduction in normalised local shear stress with normalised distance from pile base.

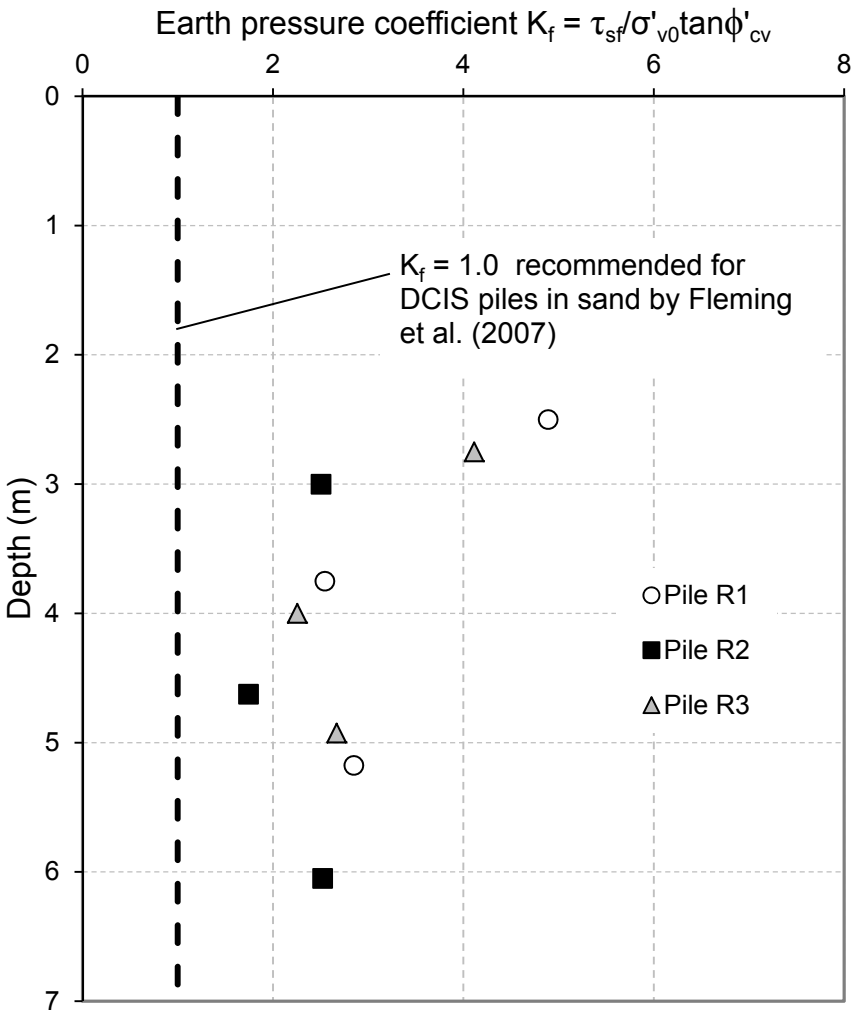

Fig. 15. Lateral earth pressure coefficients at failure.

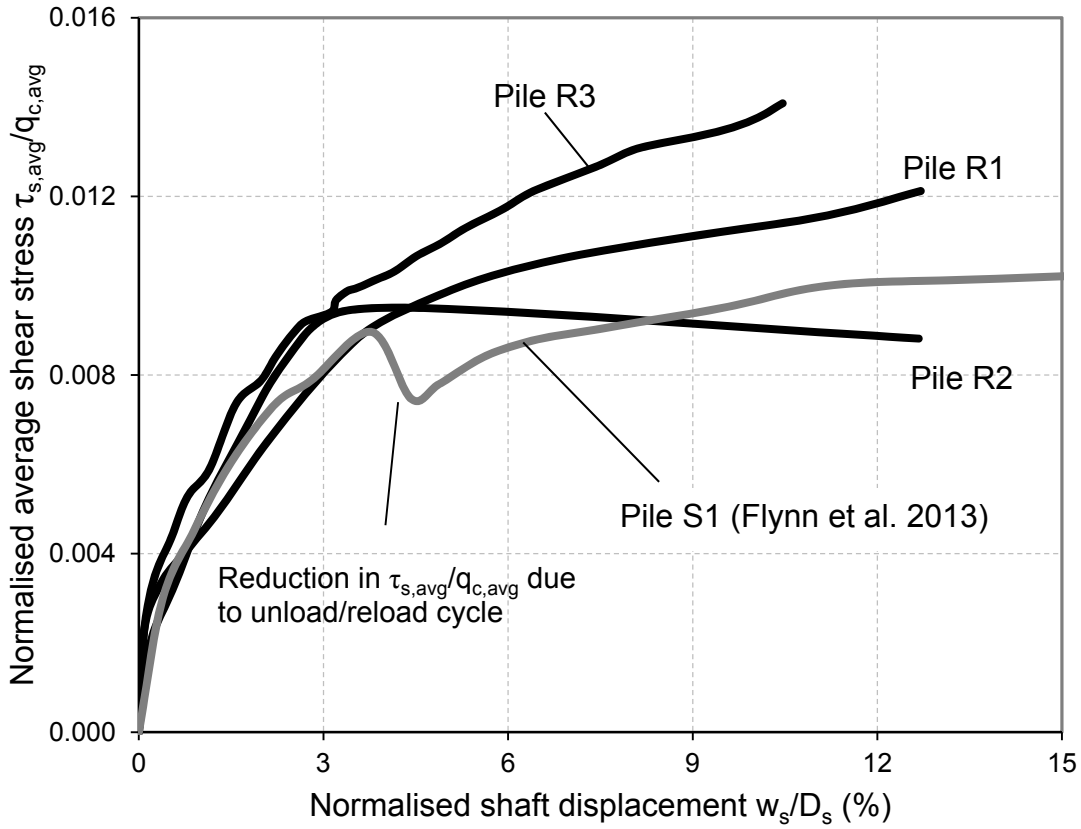

Fig. 16. Normalised average shear stresses.

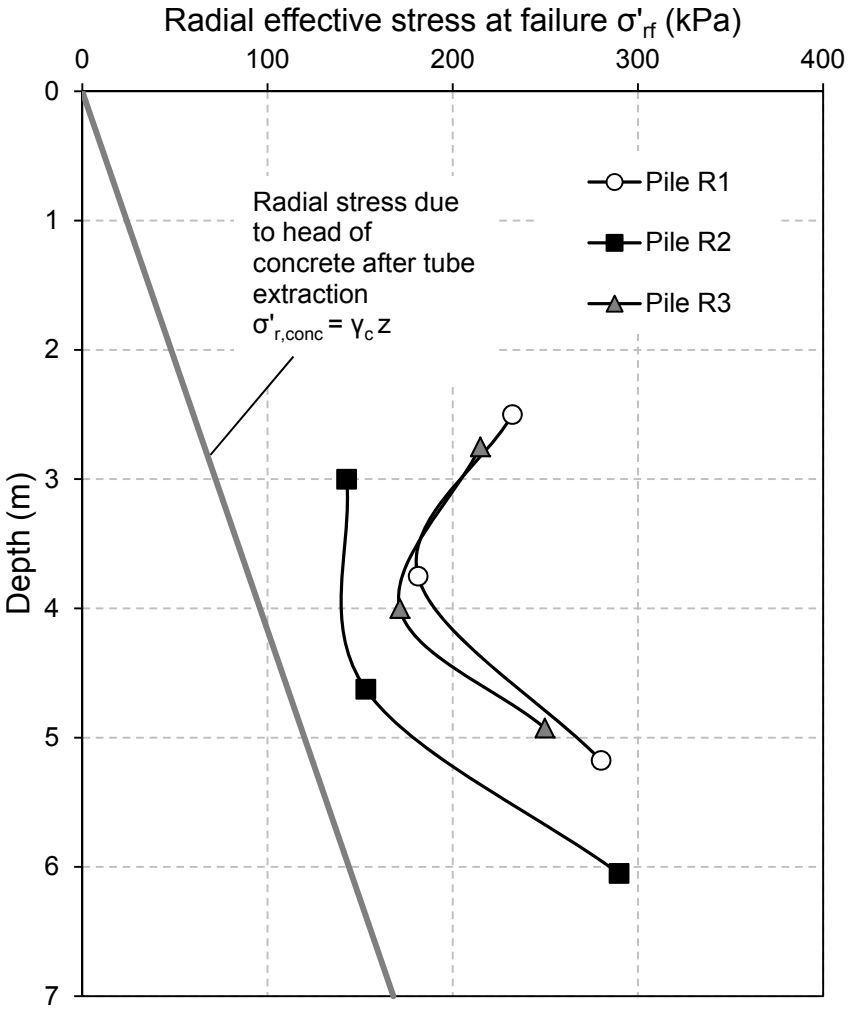

Fig. 17. Distribution of radial effective stress at failure.

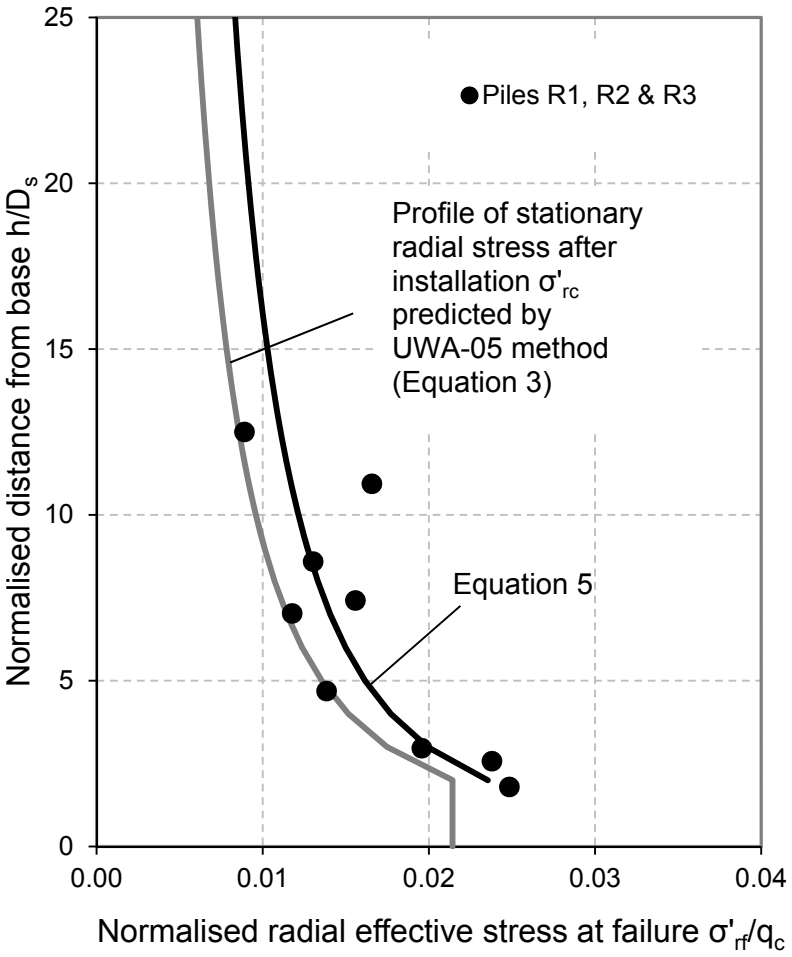

Fig. 18. Comparison of normalised radial stresses at failure with profile of normalised radial stress after installation predicted by UWA-05 method.